Sensors and Actuators B 242 (2017) 1065–1072

Contents lists available at ScienceDirect

Sensors and Actuators B: Chemical

journal homepage: www.elsevier.com/locate/snb

Photonic crystal fiber interferometer coated with a PAH/PAA nanolayer as humidity sensor

Diego Lopez-Torres[a,*], Cesar Elosua[a,b], Joel Villatoro[c,d], Joseba Zubia[c], Manfred Rothhardt[e], Kay Schuster[e], Francisco J. Arregui[a,b]

[a] Nanostructured Optical Devices Laboratory, Electric and Electronic Engineering Department, Public University of Navarre, Edif. Los Tejos, Campus Arrosadía, 31006 Pamplona, Spain
[b] Institute Of Smart Cities (ISC), Centro Jerónimo de Ayanz, Campus Arrosadia, 31006 Pamplona, Spain
[c] Department of Communications Engineering, Escuela Técnica Superior de Ingeniería de Bilbao, University of the Basque Country, Bilbao 48049, Spain
[d] IKERBASQUE, Basque Foundation for Science, Bilbao, Spain
[e] Leibniz Institute of Photonic Technology (IPHT), Albert-Einstein-Strasse 9, 07745 Jena, Germany

ARTICLE INFO

Article history:
Received 30 June 2016
Received in revised form
21 September 2016
Accepted 23 September 2016
Available online 25 September 2016

Keywords:
Photonic crystal fiber
Interferometer
Layer-by-layer nanoassembly
Humidity sensor
Fast Fourier transform

ABSTRACT

In this paper, an optical fiber interferometric humidity sensor is presented. The device consists of 1 cm-long segment of photonic crystal fiber (PCF) spliced to standard single mode fibers (SMFs), forming an interferometer: the two collapsed interfaces between PCF and SMF segments produce the excitation and recombination of core and cladding modes. The latter interact with a poly(allylamine hydrochloride) (PAH) and poly(acrylic acid) (PAA) polymeric nanocoating deposited on the PCF by the well-established layer-by-layer nano assembly (LbL) technique. Humidity modifies the index of the polymeric nanolayer which in turns alters the cladding modes along the PCF segment and causes a detectable shift to the interference pattern. A study of different nanocoting thicknesses is presented in order to obtain the best possible sensibility for the sensor. Furthermore, the interrogation of the humidity sensor is presented not only by the conventional study of the spectrum shift amplitude, but also making use of the Fast Fourier Transform (FFT), which yields a linearization of the device response. The sensor here presented is reproducible, can resolve 0.074% of relative humidity (RH) and operates in the 20–95% RH range. Moreover, it exhibits response time of 0.3 s, a negligible cross sensitivity to temperature as well as long term stability.

1. Introduction

A large number of papers have been published in the field of optical fiber sensors in the last decades [1–4]. These devices can benefit from advantage of the electromagnetic immunity, light weight, low transmission losses in the communication windows, low cost or wavelength multiplexing. The utilization of optical fiber sensors for measurement of different magnitudes such as temperature [5], humidity [6], gases [7] or pHs [8] has been described by different authors in the literature using a wide range of interrogation techniques i.e. interferometry, long-period gratings or resonances.

In the past decade, new optical fibers have been developed in order to get lower nonlinearity, lower attenuation, and unique wave-guiding properties. This is the case of Photonic Crystal Fibers (PCFs), proposed in 1995 by Russell et al. [9] which contain arrays of tiny air holes along their structure allowing the development of new applications and the fabrication of new optical fiber sensors. If a portion of PCF is spliced between two segments of single mode fibers, then a Photonic Crystal Fiber Interferometer (PCF-I) is obtained. In such devices, the fundamental mode guided in the core of the single mode fiber, when reaches the interface with the PCF, can excite cladding modes of the PCF. In this manner, the light signal is divided in two components: one traveling through the core of the PCF and the other one along its cladding. At the end of the PCF segment, the both modes are recombined in the core of the second

Abbreviations: LbL, layer-by-layer; PCF, photonic crystal fiber; KOH, potassium hydroxide; PAH, poly(allylamine hydrochloride); PAA, poly(acrylic acid); RH, relative humidity; FFT, fast Fourier transform; OSA, optical spectrum analyzer; SNR, signal to noise ratio.

* Corresponding author.
E-mail addresses: diego.lopez@unavarra.es (D. Lopez-Torres), cesar.elosua@unavarra.es (C. Elosua), agustinjoel.villatoro@ehu.eus (J. Villatoro), joseba.zubia@ehu.es (J. Zubia), manfred.rothhardt@leibniz-ipht.de (M. Rothhardt), kay.schuster@leibniz-ipht.de (K. Schuster), parregui@unavarra.es (F.J. Arregui).

http://dx.doi.org/10.1016/j.snb.2016.09.144
0925-4005/

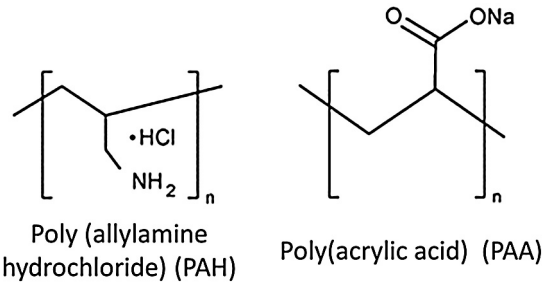

Fig 1. Chemical structures of the hydrogels (PAH/PAA).

single mode fiber: it produces an oscillatory spectral response of an interferometer. These devices are used to implement sensors: the transduction is based on depositing a sensing material along the PCF segment: the cladding modes are affected by the external medium surrounding the PCF and, therefore, the interferometric pattern is altered.

In order to create a humidity fiber sensor, the utilization of PCF-I combined with an agarose coating sensitive to humidity and deposited by dip-coating has been presented in previous works [10]. However, due to the limitations of the deposition technique, these sensors present some drawbacks such as the reproducibility in the fabrication of the nanocoating as well as the limitation to control the thickness of the coating on the nanometer scale [11].

The current work proposes the use of two polymers (poly(allylamine hydrochloride) (PAH) and poly(acrylic acid) (PAA)) deposited by layer-by-layer nanoassembly (LbL) on a Photonic Crystal Fiber Interferometer (Fig. 1 shows the chemical structures of the hydrogels) (PAH/PAA). Based on [12], absorption (swelling and deswelling) is the mainly mechanism of interaction between water molecules and [PAH/PAA] nanofilm. At lower humidity (RH values up to ≈60%), the nanofilm shows a low swellability and it can be physically explained by strong interchain H-bonding between COOH groups. At higher humidity, however, water penetrates the structure, mitigates interchain H-bonding, and permits rapid swelling as the COOH groups ionize and are forced apart. Working at the nanometer scale with the humidity sensing coating should overcome the limitations seen in previous works. Furthermore, since the thickness of the coatings is below the penetration depth of the evanescent field, the sensing coating cannot be considered as an infinitum medium. Due to this, besides the sensitivity to the refractive index of the sensing coating, the sensitivity to the coating thickness could also play an important role [13].

In addition, the studied humidity sensors were interrogated not only studying the spectrum shift but also making use of the Fast Fourier Transform (FFT) for monitoring the spectrum phase variations. The FFT is calculated by the software MATLAB through the command fft. A script in MATALB was programmed in order to obtain the phase sensor response using the recorded data obtained by the OSA and the command mentioned above (fft). This method does not depend of the signal amplitude and also avoids the necessity of tracking the wavelength evolution in the spectrum; moreover, it is applicable to networks that require narrow band sensors, allowing high multiplexing rates. The proposed sensor is characterized following the spectral shift and FFT approaches, comparing them in terms of sensitivity and linearity [14].

To our knowledge, this is the first time that a nanocoating has been deposited by means of LBL on a PCF-I to achieve a humidity sensor and moreover, the first time FFT is used to characterize this type of configuration.

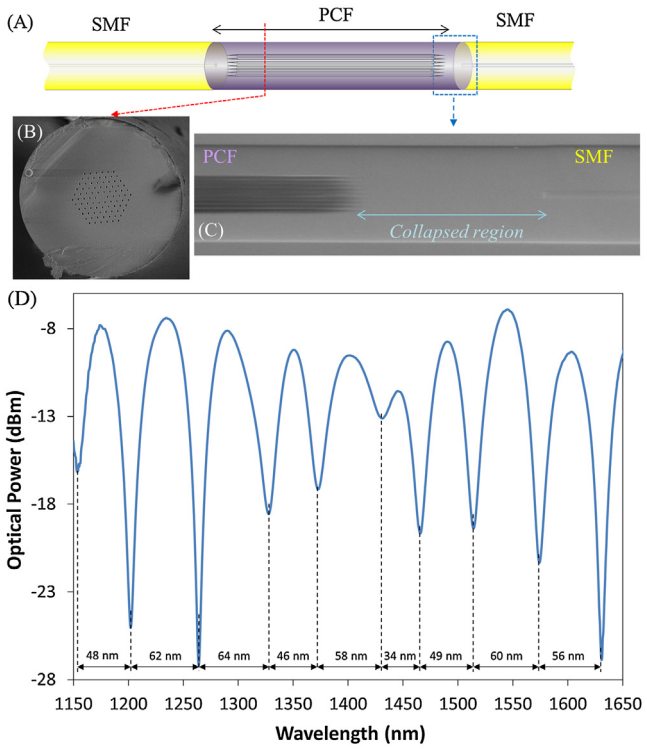

Fig. 2. (A) Schematic representation of the photonic crystal fiber interferometer (PCF-I); (B) Micrograph of the PCF-SMF juntionc showing the collapsed region of the PCF; (C) Cross section of the PCF used to build up the interferometer; (D) Transmission spectrum of the PCF-I.

2. Experimental details

2.1. Chemical reagents

Two different polymers have been used for the construction of the nanocoating: poly(allylamine hydrochloride) (PAH) (Mw ~15,000) and poly(acrylic acid) (PAA) (Mw ~15,000) 35 wt% solution in water. The cleaning and the generation of a superficial electrical charge on the optical fiber were performed by 10% Potassium Hydroxide (KOH) solutions. The pH of the different mixtures was measured by an electronic pH-metter (Crimson INC). The acidity of the polymeric solutions was adjusted to pH 4.4 by Hydrochloridric acid (HCl) and Sodium Hydroxide (NaOH). The entire set of reagents were supplied by Sigma–Aldrich and they were used without further purification. All solutions were prepared using ultrapure water with a resistivity of 18.2 MΩ cm (Diamond RO D12671).

2.2. Construction of the nanocoating

Prior to the deposition of the nanocoating, one centimeter of standard PCF (LMA-8 Crystal Fiber A/S) was spliced to Corning SMF-28 (standard fiber optic) with a conventional splicing machine. The splicing was carried out in such a way that the voids of the PCF collapsed completely over a short region (generally less than 300 micrometers long) [15]. At this point, the PCF-I was attached to a U-shaped holder in order to prevent undesired bending or possible breakages and, in addition, to facilitate the coating deposition. Fig. 2 shows a schematic representation of the resulting interferometer, detailing the PCF microstructure and the collapsed region interface.

The technique used for the deposition of the humidity sensitive coating was LbL nanoassembly technique. The method was proposed by Decher [16] as a simple and automatable method

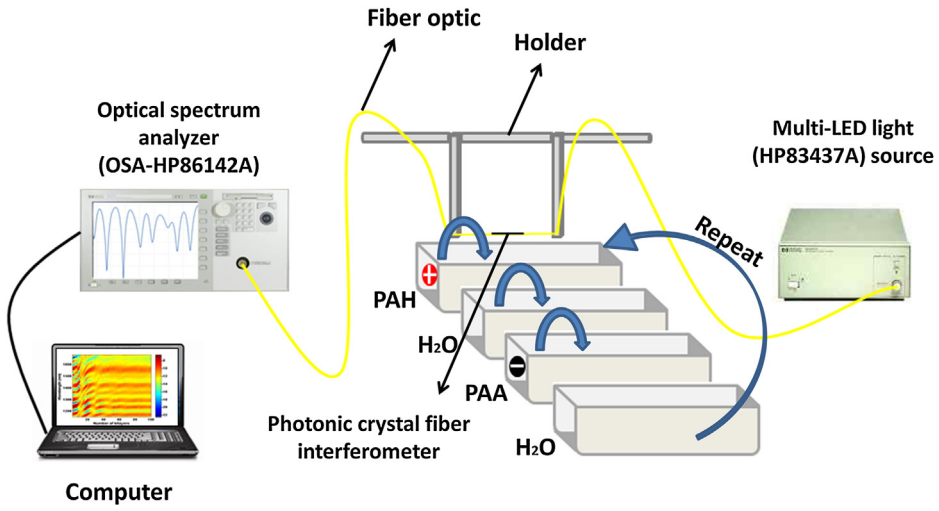

Fig. 3. Transmission set up used to monitor de deposition process based on LbL nano assembly method.

to fabricate films at the nanometer scale. LbL technique consists of the assembly of oppositely electrically charged polyelectrolytes (polycation and polyanion respectively) forming a bilayer [17]. LbL procedure is not limited by the shape or the size of substrates, which a remarkable feature for optical fiber sensors [18]. First of all, PCF-I was immersed for ten minutes into a 1 M potassium hydroxide (KOH) aqueous solution in order to induce a negative electrical superficial charge. Thereafter, the PCF-I was cleaned up in ultrapure water. The nanocoating was prepared dipping the PCF alternatively into the 10 mM polyelectrolyte solutions: first, the fiber was immersed into the polycationic solution (PAH) for two minutes and then it was washed with ultrapure water for 1 min to remove the not properly assembled chains; then, the device was dipped into the polyanionic (PAA), rinsing it again with ultrapure water for another minute. In this manner, a bilayer with the structure [PAH/PAA] was conformed. This process was repeated as many times as required. The method was automated by using a robotic arm (acquired from Nadetech Innovations S.L.), ensuring its reproducibility.

2.3. Characterization setup

The transmission setup used in this work is shown in Fig. 3. The transmission configuration has advantages when it is compared with the reflection one used in previous works [19,20]: the collapsed voids interface cannot be contaminated by dust or unwanted particles causing an erroneous measurement; moreover, the use of the fiber optic circulator is not required. The PCF sensor device was interrogated with a multi-LED light (HP83437A) source whose emission spectrum span was between 1150 and 1650 nm allowing the spectra behavior of the PCF interferometer to be studied in a higher spectra range; the sensing signal was acquired by an optical spectrum analyzer (OSA-HP86142A). To calculate the interferometric response, the signal obtained with a SMF pigtail connecting the light source and the spectrometer was considered as reference. Once the interferometer was included to the setup, the interferometric response was evaluated comparing the different signals with the reference. In this manner, changes in the interferometric pattern were observable. This set up was used to monitor both the growth of the nanocoating and its response with RH changes in terms of wavelength shifts.

The influence of the length of the PCF segment on the fringe spacing of a transmission-type PCF interferometer was investigated [21]. It was shown an inversely proportional relation between the fringe spacing and the length of the PCF section. In order to facilitate the study of the PCF-I humidity response and to increase the measurement range of relative humidity, a large fringe spacing for the interferometer was required. The length of the PCF was 10 mm: the resulting averaged fringe spacing was ~53 nm (see Fig. 2D), which allowed the construction process to be optimized in terms of maximum sensitivity as well as to characterize the sensor.

3. Study of thickness effect on the sensor sensitivity

The fabrication of the nanocoating was monitored using the setup described in Fig. 3. As it was mentioned in the introduction section, the evanescent field along the PCF section interacts with the surrounding media a distance known as penetration depth, which is below 1 μm. The thickness of the sensing coating deposited by LbL method is in the nanometrical scale: as more bilayers get deposited, their interaction with the evanescent field changes, and in this manner, so does the interferometric pattern. In terms of the spectral shape, it was observed a red shift as the number of bilayers increased. Furthermore, the sensing coating behaves as and hydrogel, so that the interaction between [PAH/PAA] nanofilm and water molecules causes the effect of swelling and deswelling. Consequently, an increase in the nanofilm thickness occurs when the relative humidity is increased [12]. And according to Fig. 5, an increase in the nanofilm thickness results in a redshift (always working below the penetration depth of the evanescent field, where the effect of the thickness change plays a dominant role with respect to the contribution of the refractive index variation). Thus, a decrease in the nanofilm thickness gives a blueshift. Therefore, the construction process should show an optimal point at which variations in RH would produce significant spectral shifts: actually, this point would show the highest slope (in terms of spectral shift).

The effect of the nanocoating thickness (firstly expressed as the number of bilayers) was studied by monitoring the interferometric pattern for a 100 bilayers nano construction. The resulting spectrum after the deposition of each bilayer was recorded: all of them are displayed in 2D graphs (Fig. 4A): every spectrum is represented in the vertical axis, and their respective magnitudes (expressed in dB) are indicated by a color map. It can be observed that there are 3 sections along the construction process that show different slopes in terms of spectral shift: they are marked with dashed squares in Fig. 4A. Actually, the slope gets lower as the number of bilayers is increased: in fact, there is almost no shift once 60 bilayers are deposited. It is a consequence of the coating thickness: above 60 bilayers, this parameter is thicker than the penetration depth of

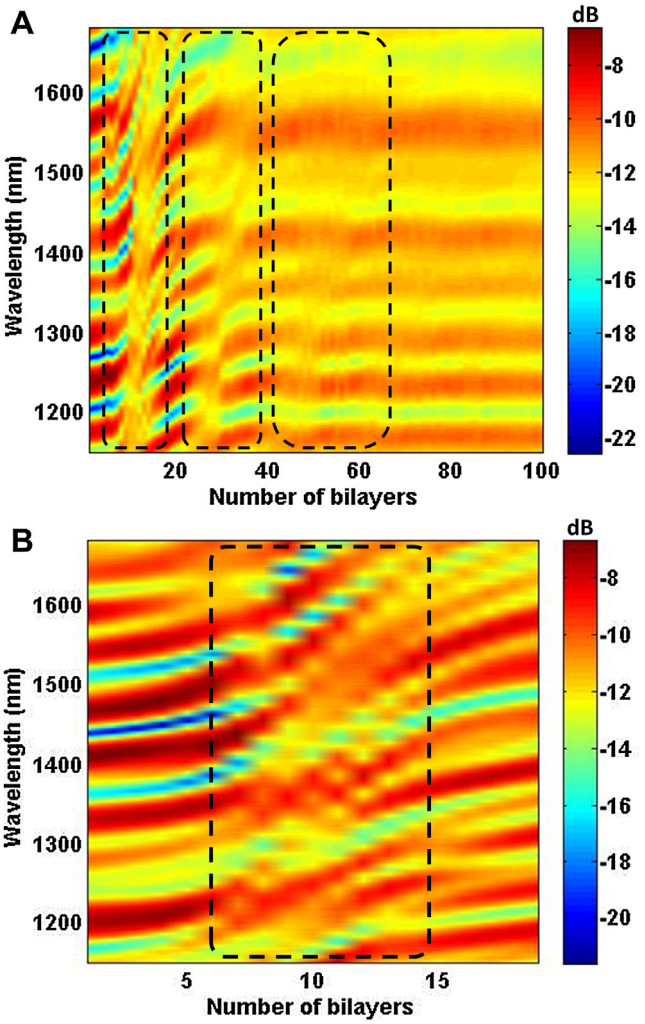

Fig. 4. (A) Transmission spectra that were recorded after the deposition of every single layer: the dashed squares highlight the areas with a remarkable spectral red shift; (B) Detailed representation of the spectra registered from the deposition of the first 20 bilayers: the dashed line frames the spectra that show a significant red shift (For interpretation of the references to color in this figure legend, the reader is referred to the web version of this article.).

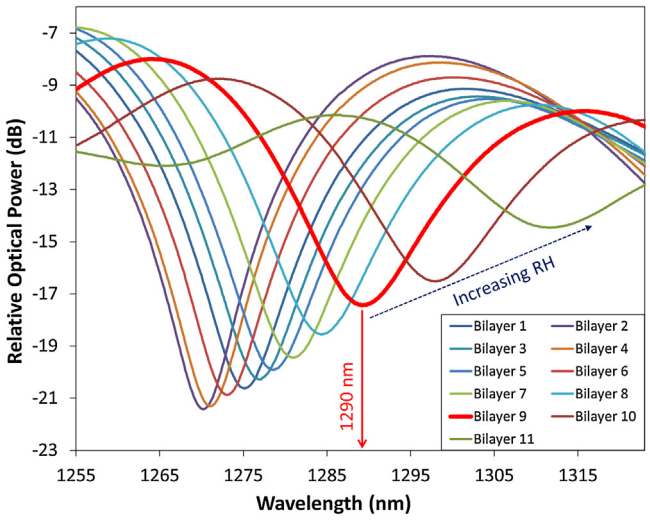

Fig. 5. (A) Spectral red shift observed along the construction process from 1225 nm and 1325 nm. After 9 layers are deposited, the transmission valley is centered at 1290 nm: its spectral shift when RH is increased is supposed to show the optimal sensitivity, following the trending pointed in the graph (For interpretation of the references to color in this figure legend, the reader is referred to the web version of this article.).

the evanescent, so that any increase above this point produces no variation in the interaction between the coating and this propagating mode. What is more, the evanescent field decays exponentially from the cladding, which explains why the slope of the shift is lower as more layers are deposited. Fig. 4B displays a detailed representation of the spectra from the first 20 bilayers: it can be observed that for 10 bilayers the slope is maximum, so that to get the optimal sensitivity, the construction process was to be stopped for 9 bilayers. Fig. 5 shows in detail the spectral shift for the transmission valley initially located at 1270 nm, verifying that for that number of bilayers the sensitivity should be optimal. Therefore, once another sensor was prepared with just 9 bilayers, the location of the spectral valley to monitor was 1290 nm. In order to not affect the coating deposition, the thickness of the sensor was only measured at the end of the fabrication process. Due to this, in our work we only measured the thickness of the coating at the end of the process, the sensor with 9 bilayers. The thickness of the deposited coating was measured by a Scanning Electronic Microscope: the resulting value was 240 ± 20 nm (below the penetration depth of the evanescent field) and, moreover, the images shown a uniform coating morphology (Appendix A Supplementary data, Fig. S1 in the online version, at http://dx.doi.org/10.1016/j.snb.2016.09.144). These data are in accordance with [22], where the thickness of the PAH/PAA polymeric coating is estimated as a function of the number of bilayers, from 0 to 100 bilayers.

4. Results and discussion

The relative humidity (RH) response of a PAH/PAA nanocoated PCF-I was studied with the set up shown in Fig. 6: the sensor was placed inside a climatic chamber (Angelantoni, CH 250). Several experiments were implemented changing the relative humidity from 20% to 95% at $25\,^{\circ}C \pm 2\,^{\circ}C$ at room atmospheric pressure. The sensor response was firstly characterized following the red shift of the transmission valley that shown the highest sensitivity: as it was mentioned in the previous section, it was located at 1290 nm once the construction process was over. This type of characterization is typically performed for sensors based on interferometers, but it has two remarkable drawbacks: on one hand, the wider the transmission valley (or peak) is, the less accurate is its wavelength location; on the other hand, in the case of several peaks are recorded, only the information of one of them is used, so the rest of the spectrum becomes useless, reducing the potential robustness of the sensor. In this context, it is possible to take advantage of the whole spectrum by applying an analysis based on FFT: as an interferometric response, the magnitude of the resulting FFT spectrum is not supposed to change, but the phase one should show the spectral shifts. In this manner, the sensor response can be studied following the most significant components of the phase spectrum obtained from FFT analysis of the sensor signal. Another relevant feature is that SNR is not as restrictive as in the case of wavelength shift based measurements and moreover, it is applicable to narrow band sensors, which allows working with high multiplexation rates [23].

In order to compare the wavelength shift and the FFT methods, the sensor was exposed to 20%–95% increasing/decreasing cycles (temperature was kept constant at $25\,^{\circ}C$). The spectra were recorded every minute, and they were processed following both approaches: the results are plotted in Fig. 7. As it can be observed in Fig. 7A, there is no a linear relationship between the wavelength shift and the RH: the total shift is 61 nm, which is higher than the one reported in previous works [21] (56 nm). The relationship between the shift and RH is not lineal along the entire range of

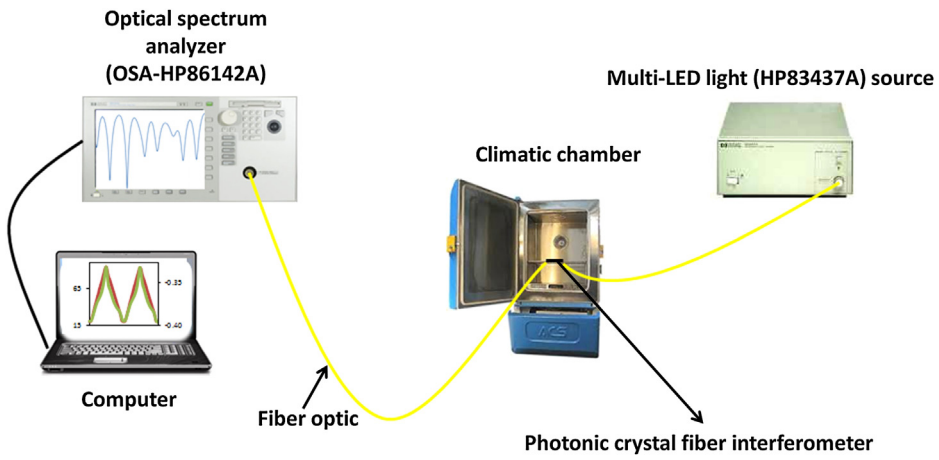

Fig. 6. Set up used to study the response of the sensor to RH variations: it is located inside a climatic chamber where humidity and temperature are controlled.

RH: for lower humidity values (20%–75%), an almost linear behavior linear behavior is observed, with a sensitivity of 0.29 nm/% RH; in contrast between 75%–95%, the response is exponential, with an estimated sensitivity of 2.35 nm/% RH. The resolution for each RH segment is 0.21% RH and 0.025% RH respectively and the humidity resolution for the entire range, 20–95% RH, is 0.074% RH. Other feature of the sensor is that the signal is very stable when the RH is constant at 20% (at the beginning and at the end of the measurement, as well as between every cycle). In order to clarify these dates, Table 1. compares the [PAH/PAA] PCF-I resolution with the earlier devices published [21] and confirms that the total resolution of the [PAH/PAA] PCF-I resolution is the highest, to our knowledge, for a relative humidity change from 20% to 95% RH.

The results obtained when applying FFT are displayed in Fig. 7B. The response with this method is more linear and less noisy than the study of the spectrum shift focused on a specific peak. This improvement can be associated to work only with the most significant component of the FFT module. FFT technique can be applied due to the existence of a series of periodic maxima and minima in the transmission spectra of the PCF-I, but it is not ideally periodic; moreover, no-linear components appear in the spectrum. The interferometric response changes due to phase variations of the pattern: in the case of wavelength shift, they follow a non linear mathematical expression, but for FFT, just the phase component of this expression is considered, which is linear (the non linear components of the spectrum produce the deviation from the linear approach). Considering the response as linear (in the range 20%–95% RH), the sensitivity is 0.86 mrad/% RH (0.16°/% RH) and the total phase shift is 0.065 rad (12°).

The resulting characterizations for both approaches are also plotted in Fig. 8A (wavelength shift) and 8 B (phase shift): in both graphs, the response registered with increasing and decreasing RH is displayed in order to check hysteresis. In the case of the wavelength shift based analysis, the remarked non linear response for RH values above 80% is observable; on the contrary, when the FFT analysis is applied, the behavior of the sensor is more linear. Two fitting lines have been calculated in order to confirm this assumption. The R^2 of the wavelength analysis (Fig. 8A) is 0.992 when the relative humidity is increased from 20% to 75% RH and 0.9047 when the relative humidity is increased from 75% to 95% RH. For the case of FFT analysis (Fig. 8B), the R^2 is 0.9936 in the first range and 0.9862 in the second range. In both cases, the R^2 is higher when the FFT is applied. This difference is because the shift of the interferometric pattern depends linearly on the phase component of its FFT spectrum. It is also remarkable that the hysteresis of the sensor is below 5%.

In order to study the influence of temperature in the $[PAH/PAA]_9$ nanocoated PCF-I, cycles with different temperatures (from 15 °C to 45 °C) were performed. Fig. 9 shows the phase variation along these cycles. The sensitivity of the PCI interferometer in the range of 15 °C–45 °C is $5.23 \times 10{-}5$ rad/°C (0.003°/°C). This sensitivity (0.003°/°C) is much lower than the sensitivity obtained in the humidity cycles (0.18°/% RH): it can be concluded that the PCF-I sen-

Table 1
Comparison between [PAH/PAA] PCF-I resolution and earlier devices published [21] where a humidity sensor based on an Agorose-coated was carried out.

PAH/PAA PCF-I (OSA resolution: 0.06 nm)	PAH/PAA PCF-I (OSA resolution: 0.01 nm)	Earlier published, Ref [21] Agarose (OSA resolution: 0.01 nm)
Total wavelength for a RH change of 75% RH → 61 nm	Total wavelength for a RH change of 75% RH → 61 nm	Total wavelength for a RH change of 60% RH → 56 nm
Resolution in the lineal range for a RH change of 55% RH → 0.21% RH	Resolution in the lineal range for a RH change of 55% RH → 0.035% RH	Resolution in the lineal range for a RH change of 40% RH → 0.017% RH
Resolution in the lineal range for a RH change of 20% RH → 0.025% RH	Resolution in the lineal range for a RH change of 20% RH → 0.004% RH	Resolution in the lineal range for a RH change of 20% RH → 0.007% RH
Total resolution for a RH change of 75% RH → 0.07% RH	Total resolution for a RH change of 75% RH → 0.01% RH	Total resolution for a RH change of 60% RH → 0.01% RH

The resolution of each RH segment is determined as follows:

1. First of all, we calculate the wavelength shift in each segment (~16 nm for the first area, humidity values from 20% to 75% RH and ~45 nm for the second area, humidity values from 75% to 95% RH).
2. Secondly, we divide these wavelength shifts by the relative humidity range of each segment. In the first case, 55% RH (from 20% to 75% RH) and in the second case 20% RH (from 75% to 95% RH). In this manner, we obtain the sensitivity of each segment: 0.29 nm/% HR and 2.35 nm/% HR.
3. Finally, we only have to divide the OSA resolution (in our case 0.06 nm) by the results of point 2. The result of this division is the resolution of each segment.

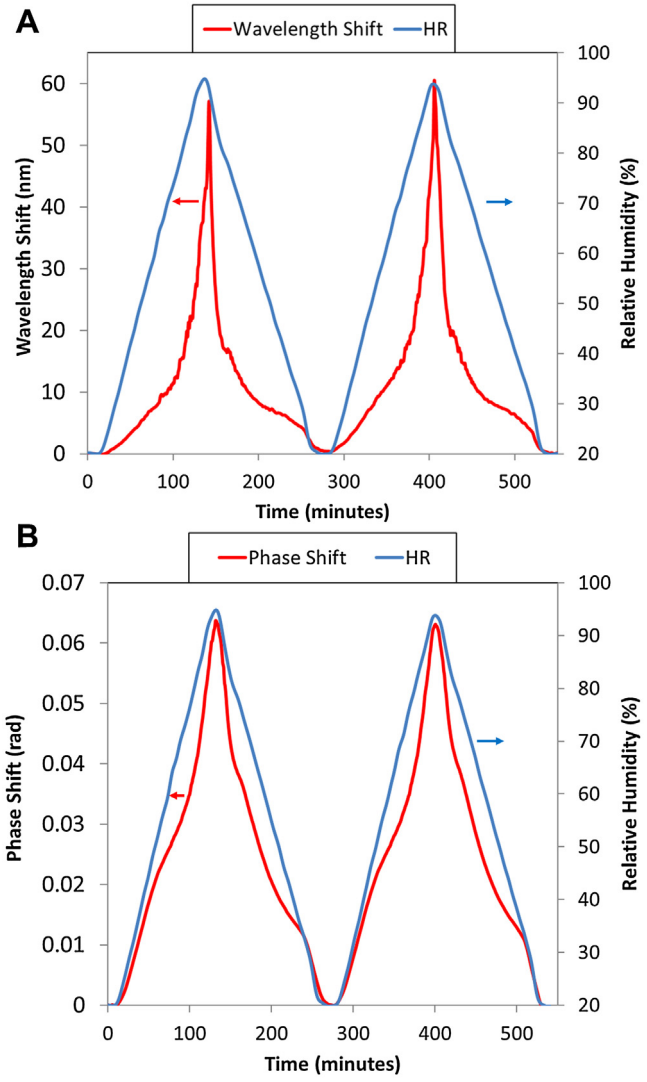

Fig. 7. Spectral shifts from the transmission valley located at 1290 nm once the deposition process was completed: (A) RH values are represented on the right hand axis, whereas the wavelength shift is indicated in the left hand one; (B) Phase shift observed once the FFT is applied to the transmission spectrum along the humidity cycles.

sor has a negligible cross correlation with temperature [24], which is a relevant feature in relative humidity sensing applications.

The kinetics of the sensor were also studied. The set up used was the same one shown in Fig. 3 but OSA was set to mode "Zero Span": in this manner, the intensity of the sensing signal at a specific wavelength (1285 nm) was monitored. Humidity changes were performed using the human breath towards the sensor. This experiment consists of inhaling and exhaling several times placing the sensor close to the mouth, so that quick RH variations are produced by breathing. The shift in the spectrum of transmission was studied at a room temperature of 20 °C and RH of 55%. Roughly, the maximum value reached by human breath exhale is 90%: therefore, the approximate range of RH in this experiment is 55%–90%. The temporal response of the sensor is shown in Fig. 10. In every cycle, the response recovered the baseline and the observed signal variations confirmed the repeatability of its response. The average response time of the PDF-I is below 300 miliseconds, whereas the recovery time was found shorter than 270 miliseconds. The test was repeated three weeks later and the results obtained were similar (see Fig. 10), so that the temporal stability of the sensor is verified.

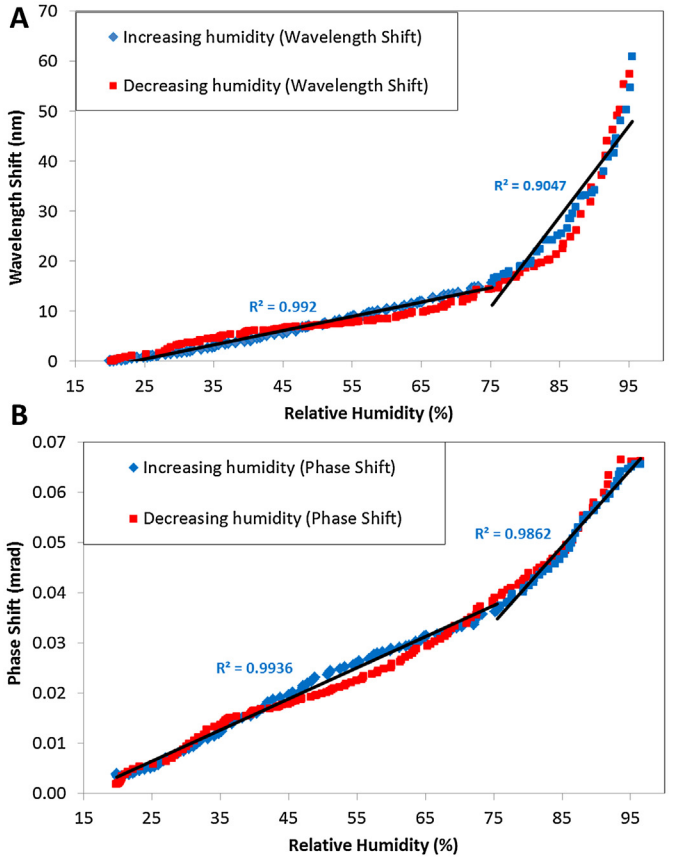

Fig. 8. Characterization of the sensor response as a function of the relative humidity expressed in (A) wavelength shift and (B) FFT phase shift.

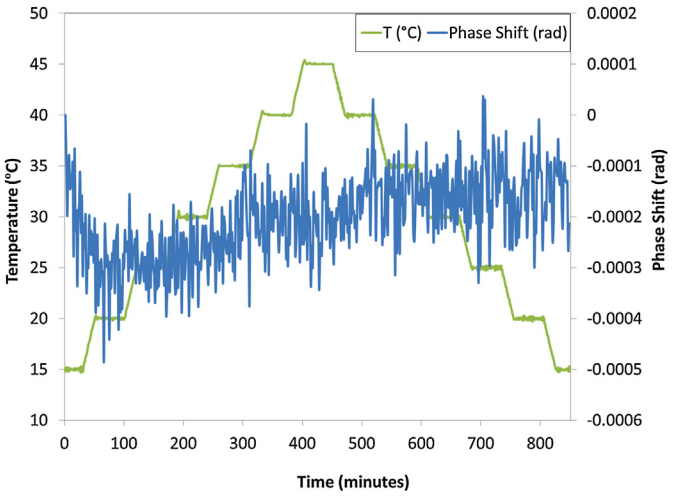

Fig. 9. Study of the effect of temperature on the phase shift.

5. Conclusions

A sensor based on PCF-I to measure RH is presented in this work. The transduction is produced by the interaction of the evanescent field along the PCF section and the sensing layer coated along it, which behaves as a hydrogel. The final sensitivity of the sensor can be optimized by adjusting the thickness of the coating (following LbL method): any variation in its value produced by changes in relative humidity will produce the highest spectral shift. In any case, the total thickness of the sensing coating has to be below the penetration depth of the evanescent field to ensure an

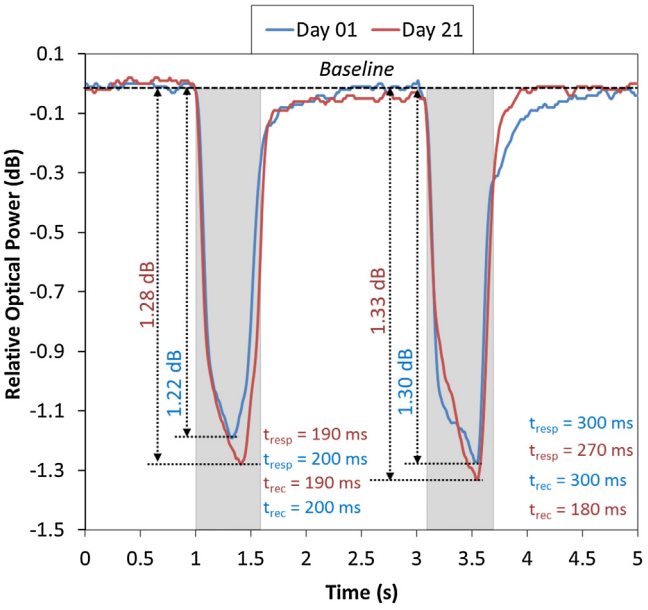

Fig. 10. Optical power at 1270 nm when the sensor is exposed to human breath. Inset, data about the signal change and kinetics are detailed; the gray areas indicate the exhalation and the white ones the inhalation.

optimal response. The sensitivity reported from PCF-I sensors prepared with hydrogels deposited with dip coating technique is lower than the obtained from the optimized sensor. The guarantied reproducibility by LbL method, as well as the just mentioned sensitivity optimization, makes this construction procedure more interesting than the traditional ones such as dip coating. Moreover, LbL technique achieves high reproducibility and a precise control in the thickness of the nanocoating allowing to work at the nanometer scale where the thickness of nanocoating is below the penetration depth of the evanescent field. At this scale the sensibility of the sensor depends mainly on the nanocoating thickness instead of the refractive index of the sensing coating.

The response of the sensor has been analyzed applying two different techniques. The first one is based on the traditional approach of following the shift of remarkable points of the interferometric spectral response, such a transmission valley. The resulting characterization is non linear for RH values above 80%. As an alternative, a method based on the FFT is proposed: the interferometric spectrum shift can be monitored by the phase component of its FFT. This approach enhances the performance of PCF-I based sensors because the resulting characterization is more linear and less noisy than the ones based on wavelength monitoring.

Temperature has a negligible effect on the sensor response and furthermore, the response of the sensor is preserved unaltered after at least 3 weeks. Regarding to its kinetics, the nanometric thickness of the coating easies the transduction, so that response and recovery times below 1 s were observed. All these features are a consequence of the synergy between the PCF-I transmission configuration, LbL method and FFT signal processing: the resulting sensor improves the results reported from previous works, making it possible to use it in applications where linear behavior is required.

Competing interests

The authors declare that they have no competing interests.

Acknowledgments

This work was supported by the Spanish Economy and Competitivity Ministry-FEDER TEC2013-43679-R. The authors would like to express their gratitude to Nadetech Inc. for the design, fabrication and tune-up of the robot used for the deposition of the nanocoatings.

References

[1] F.J. Arregui, I.R. Matías, I. Del Villar, J.M. Corres, J. Goicoechea, Optical fiber sensors based on nanostructured coatings, III Jornadas Hisp. IBERNAM-CMC2. 2015 (2006).
[2] F.J. Arregui, I.R. Matias, J.M. Corres, I. Del Villar, J. Goicoechea, C.R. Zamarreño, M. Hernáez, R.O. Claus, Optical fiber sensors based on layer-by-layer nanostructured films, Procedia Eng. 5 (2010) 1087–1090.
[3] C. Elosua, N. De Acha, I.R. Matias, F.J. Arregui, ScienceDirect luminescent optical fiber oxygen sensor following layer-by-layer method, Procedia Eng. (2014) 3.
[4] J. Ascorbe, J.M. Corres, F.J. Arregui, I.R. Matias, Optical fiber current transducer using lossy mode resonances for high voltage networks, J. Lightwave Technol. 33 (2015) 2504–2510.
[5] S.M. Chandani, N.A.F. Jaeger, Fiber-optic temperature sensor using evanescent fields in D fibers, IEEE Photonics Technol. Lett. 17 (2005) 2706–2708.
[6] M. Hernaez, D. Lopez-Torres, C. Elosua, I.R. Matias, F.J. Arregui, Sensitivity enhancement of a humidity sensor based on poly(sodium phosphate) and poly(allylamine hydrochloride), IEEE Sens. (2013) 1–4.
[7] C. Elosua, N. de Acha, M. Hernaez, I.R. Matias, F.J. Arregui, Layer-by-layer assembly of a water-insoluble platinum complex for optical fiber oxygen sensors, Sens. Actuators B: Chem. 207 (2015) 683–689.
[8] P. Zubiate, C.R. Zamarreño, I. Del Villar, I.R. Matias, F.J. Arregui, Tunable optical fiber pH sensors based on TE and TM lossy mode resonances (LMRs), Sens. Actuators B: Chem. 231 (2016) 484–490.
[9] D.M. Atkin, T.J. Shepherd, T.A. Birks, P.S.J. Russell, P.J. Roberts, Full 2-D photonic bandgaps in silica/air structures, Electron. Lett. 31 (1995) 1941–1943.
[10] J. Mathew, Y. Semenova, G. Farrell, A high sensitivity humidity sensor based on an agarose coated photonic crystal fiber interferometer, Int. Soc. Opt. Eng. 8421 (2012), 842177-842177-4.
[11] J. Mathew, Y. Semenova, G. Farrell, Effect of coating thickness on the sensitivity of a humidity sensor based on an agarose coated photonic crystal fiber interferometer, Opt. Express 21 (2013) 6313–6320.
[12] K.E. Secrist, A.J. Nolte, Humidity swelling/deswelling hysteresis in a polyelectrolyte multilayer film, Macromolecules (2011) 2859–2865.
[13] F.J. Arregui, Sensors Based on Nanostructured Materials, New York (2009).
[14] D. Leandro, M. Bravo Acha, A. Ortigosa, M. Lopez-Amo, Real-time FFT analysis for interferometric sensors multiplexing, J. Lightwave Technol. 8724 (2015) 1.
[15] J. Villatoro, M.P. Kreuzer, R. Jha, V.P. Minkovich, V. Finazzi, G. Badenes, V. Pruneri, Photonic crystal fiber interferometer for chemical vapor detection with high sensitivity, Opt. Express 17 (2009) 1447.
[16] G. Decher, Fuzzy nanoassemblies: toward layered polymeric multicomposites, Science 277 (1997) 1232–1237.
[17] F. Surre, W.B. Lyons, T. Sun, K.T.V. Grattan, S. O'Keeffe, E. Lewis, C. Elosua, M. Hernaez, C. Barian, U-bend fibre optic pH sensors using layer-by-layer electrostatic self-assembly technique, J. Phys. Conf. Ser. 178 (2009) 012046.
[18] D. Lopez-Torres, C. Elosua, M. Hernaez, J. Goicoechea, F.J. Arregui, From superhydrophilic to superhydrophobic surfaces by means of polymeric layer-by-layer films, Appl. Surf. Sci. 351 (2015) 1081–1086.
[19] J. Mathew, Y. Semenova, G. Farrell, Photonic crystal fiber interferometer for dew detection, J. Lightwave Technol. 30 (2012) 1150–1155.
[20] J. Mathew, Y. Semenova, G. Farrell, Relative humidity sensor based on an agarose-infiltrated photonic crystal fiber interferometer, IEEE J. Sel. Top. Quantum Electron. 18 (2012) 1553–1559.
[21] J. Mathew, Y. Semenova, G. Farrell, Experimental demonstration of a high-sensitivity humidity sensor based on an agarose-coated transmission-type photonic crystal fiber interferometer, Appl. Opt. 52 (2013) 3884–3890.
[22] C.R. Zamarreño, M. Hernáez, I. Del Villar, I.R. Matías, F.J. Arregui, Optical fiber pH sensor based on lossy-mode resonances by means of thin polymeric coatings, Sens. Actuators B: Chem. 155 (2011) 290–297.
[23] S. Rota-Rodrigo, R. Pérez-Herrera, A. Lopez-Aldaba, M.C. López Bautista, O. Esteban, M. López-Amo, Nanowire humidity optical sensor system based on fast Fourier transform technique, in: H.J. Kalinowski, J.L. Fabris, W.J. Bock (Eds.), Proc. SPIE—Int. Soc. Opt. Eng., SPIE, 2015, p. 96342H.
[24] M.F. Durstock, M.F. Rubner, Dielectric properties of polyelectrolyte multilayers, Langmuir 17 (2001) 7865–7872.

Biographies

Diego López-Torres received the M.S. degree in electrical and electronic engineering and the master's degree in communications from the Public University of Navarra

(UPNA), Pamplona, Spain, in 2013 and 2014, respectively. Since 2014, he has been working as a Researcher at the UPNA. In 2105, he obtained a scholarship from this university. His research interest includes optical fiber sensors, photonic crystal fiber and nanostructured materials.

Cesar Elosúa Aguado received his MS degree in electrical and electronic engineering from the Public University of Navarre (UPNA, Pamplona, Spain) in 2004. In the same year, he obtained a scholarship from the Science and Technology Spanish Ministry and he joined the optical fiber sensor group at UPNA. During 2008, he was a visiting Ph.D. student at the University of Limerick and at the City University of London. He became a lecturer of this department in 2009, receiving his PhD degree in the next year. His research interests include optical fiber sensors and networks, organometallic chemistry and data mining techniques.

Joel Villatoro received the M.Sc. and Ph.D. degrees in optics from the National Institute for Astrophysics, Optics, and Electronics, Puebla, Mexico, in 1995 and 1999, respectively. He is currently Ikerbasque Research Professor at the University of the Basque Country, Spain. Prior to that, he worked for the Aston Institute of Photonic Technologies (UK) and the world-famous ICFO—Institute of Photonic Sciences (Spain), among others. He is the author of nearly 100 scientific publications and of 6 patents. His contributions to his field are acknowledged by the internationally community as reflected by a large number of citations and several invited talks.

Joseba Zubia received a degree in solid-state physics in 1988 and the PhD degree in physics from the University of the Basque Country, in 1993. His PhD work focused on optical properties of ferroelectric liquid crystals. He is a full professor at the Telecommunications Engineering School (University of the Basque Country, Bilbao, Spain). He has more than 8 years of experience doing basic research in the field of plastic optical fibers. At present, he is involved in research projects in collaboration with universities and companies from Spain and other countries in the field of plastic optical fibers, fiber-optic sensors, and liquid crystals. Prof. Zubia won a special award for best thesis in 1995.

Manfred Rothhardt received his diploma degree from the Physics faculty of the Friedrich-Schiller-University, Jena, Germany in 1984. From 1984 to 1991 he was a scientific assistant in the research center of Carl-Zeiss-Jena GmbH. From 1991 to 1995 he was with Jenoptik AG leading a R&D group developing interferometric measurement systems. Since 1995 he is with Institute of Photonic Technology, Jena. His research interest includes applications of fibre Bragg gratings and planar lightwave circuits in sensors, biophotonics, fiber lasers and telecommunication.

Kay Schuster holds the group leader position of the Optical Fibres Technology Group within the Fibre Optics Division of the Leibniz Institute of Photonic Technology (IPHT Jena). He obtained his PhD in inorganic chemistry 1995 at the University of Karlsruhe (Research University). Dr. Kay Schuster is engaged for many years in preparation of specialty fibres, based on heavy metal oxide glasses, chalcogenide glasses and high purity silica. The recent activities of Dr. Schuster are concentrated on design and preparation of special functionalized microstructured fibres for passive, active and remote sensing applications. Beside the fabrication of specialty microstructured fibres the group is intensively engaged in material science as well as preform and fibre manufacturing for high power fibre lasers and FBG and Raman based sensing applications. He has coauthored/authored 82 articles in refereed journals, 2 book chapters and holds 3 patents.

Francisco J.Arregui (M'01) is a Full Professor at the Public University of Navarre, Pamplona, Spain. He was part of the team that fabricated the first optical fiber sensor by means of the Layer-by-Layer assembly method at Virginia Tech, Blacksburg, VA, USA, in 1998. He is the author of around 300 scientific journal and conference publications. He has been an Associate Editor of "IEEE Sensors Journal", "Journal of Sensors" (founded by Prof, Arregui in 2007), and "International Journal on Smart Sensing and Intelligent Systems". He is also the editor of the books entitled Sensors-Based on Nanostructured Materials and Optochemical Nanosensors.